THE JOURNAL OF PHYSICAL CHEMISTRY B

Article

pubs.acs.org/JPCB

Influence of Annealing on Chain Entanglement and Molecular Dynamics in Weak Dynamic Asymmetry Polymer Blends

Yu Lin,[†] Yeqiang Tan,[†] Biwei Qiu,[†] Yonggang Shangguan,*[,†] Eileen Harkin-Jones,[‡] and Qiang Zheng*[,†]

[†]MOE Key Laboratory of Macromolecular Synthesis and Functionalization, Department of Polymer Science and Engineering, Zhejiang University, Hangzhou 310027, People's Republic of China

[‡]Polymers Research Cluster, School of Mechanical and Aerospace Engineering, Queen's University Belfast, Belfast BT9 5AH, United Kingdom

Supporting Information

ABSTRACT: The influence of annealing above the glass transition temperature (T_g) on chain entanglement and molecular dynamics of solution-cast poly(methyl methacrylate)/poly(styrene-co-maleic anhydride) (PMMA/SMA) blends was investigated via a combination of dynamic rheological measurement and broadband dielectric spectroscopy. Chain entanglement density increases when the annealing temperature and/or time increases, resulting from the increased efficiency of chain packing and entanglement recovery. The results of the annealing treatment without cooling revealed that the increase of the entanglement density occurred during the annealing process instead of the subsequent cooling procedure. Annealing above T_g exerts a profound effect on segmental motion, including the transition temperature and dynamics. Namely, T_g shifts to higher temperatures and the relaxation time (τ_{max}) increases due to the increased entanglement density and decreased molecular mobility. Either T_g or τ_{max} approaches an equilibrium value gradually, corresponding to the equilibrium entanglement density that might be obtained through the theoretical predictions. However, no obvious distribution broadening is observed due to the unchanged heterogeneous dynamics. Furthermore, side group rotational motion could be freely achieved without overcoming the chain entanglement resistance. Hence, neither the dynamics nor the distribution width of the subglass relaxation (β- and γ-relaxation) processes is affected by chain entanglement resulting from annealing, indicating that the local environment of the segments is unchanged.

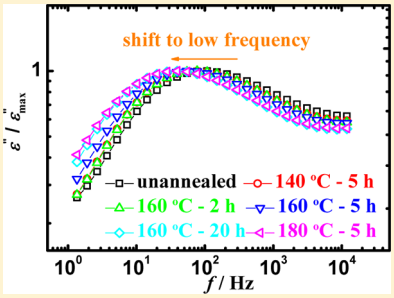

1. INTRODUCTION

It is well established that the structure−property relationship of polymer blends strongly depends on preparation and processing conditions, and most polymer blends that have undergone processing are far removed from their thermodynamic equilibrium. Consequently, their properties may change upon reheating and further annealing. Spin-casting is a very widely used technique for making uniform thin polymer films,[1−4] and one key issue yet to be resolved in this process is the effect of the process parameters (drying temperatures and time) on physical properties.

In recent decades, the effect of annealing on polymer material has attracted much attention from researchers.[5] In general, the focus has been on the material macroscopic performance, including the following. (i) The effect of annealing on the morphology evolution of polymer blends and copolymers.[6−11] It has been generally accepted that the component with a lower surface free energy is inclined to segregate to the surface upon annealing.[7] Recently, a co-continuous structure and an abnormal "sea−island" structure was reported during annealing in high-impact polypropylene copolymer.[12] (ii) The influence of annealing on the mechanical properties of polymer blends and copolymers, including tensile properties,[13] elasticity modulus,[9] fracture energy,[14] scratch behavior,[15] and so on. Nonuniform variation of properties was observed for different polymer blends. (iii) The effects of annealing on phase transitions and molecular motion, such as crystallization,[16−18] relaxation behavior,[19,20] viscoelastic behavior,[21,22] and so forth of polymer blends and composites. The effect of physical aging on structural relaxation,[23] volume, and enthalpy recovery[24,25] has also been widely investigated. Additionally, physical aging of polymer nanocomposites has attracted considerable scientific interest in recent years.[26,27]

As stated, in previous studies, attention has focused on the effect of annealing on the macroscopic properties of the polymer blend. To our knowledge, little effort has been made to understand exactly how the annealing process works at a molecular level and how this affects properties. It is therefore of academic importance to tackle this problem. To do this, it is necessary to track how chain entanglement density changes during high-temperature annealing in polymer blends. It is also important to determine whether the changes occur during the actual annealing process or in the subsequent cooling stage. A fundamental understanding of this area will be of great significance to practical processing operations such as spin-casting.

Received: October 5, 2012
Revised: December 17, 2012
Published: December 26, 2012

Polymer blends composed of polymethyl methacrylate/poly(styrene-co-maleic anhydride) (PMMA/SMA) with weak dynamic asymmetry are typical lower critical solution temperature (LCST) systems and have been widely investigated through dynamic rheological and small-angle laser light scattering (SALLS) measurements.[28−32] Previously, through two preparation routes, solution casting and melt blending, we have investigated the effects of molecular entanglement on molecular dynamics and phase-separation kinetics of PMMA/SMA blends by using broadband dielectric spectroscopy and SALLS.[33] As pointed out previously, only a merged $\alpha\beta$-relaxation process can be detected for the pure PMMA component at high temperatures,[33,34] and the β-relaxation of SMA cannot be observed in the temperature and frequency ranges investigated. A 50/50 composition by weight was adopted in this study in order to distinguish the effect of annealing on the α- and β-relaxations of PMMA/SMA blends.

In this study, PMMA/SMA blends were annealed at various temperatures above the glass transition temperature (T_g) for different times. The effect of annealing on chain entanglement density and molecular dynamics of these PMMA/SMA blends was investigated via a combination of dynamic rheological measurements and broadband dielectric spectroscopy.

2. EXPERIMENTAL SECTION

2.1. Materials and Sample Preparation. PMMA (IF850, $M_w = 8.1 \times 10^4$, $M_w/M_n = 1.9$, LG Co. Ltd., South Korea) and SMA (210, $M_w = 2.6 \times 10^5$, $M_w/M_n = 3.7$, SINOPEC Shanghai Research Institute of Petrochemical Technology, China) with a MA content of 10 wt % were supplied as commercial products. PMMA/SMA blends with a 50/50 wt/wt composition were dissolved in methyl ethyl ketone (MEK, C_4H_8O, boiling point T_b = 80 °C) at 10% by weight to form a clear and uniform solution. The solution was then cast on to flat glass Petri dishes held at 35 °C. After solvent evaporation at 35 °C for 1 day, the film samples were further dried at 50, 70, 90, 110, and 130 °C successively in a vacuum oven for at least 5 days to remove residual solvent. It is necessary to dry the films above T_g of the system to allow complete evaporation of the solvent. This was checked gravimetrically by taking the weight of the films to constant weight and further verified by thermogravimetry analysis (TGA) results (shown in the Supporting Information). The film thickness was about 100 μm. The films for the annealing experiments were annealed in a vacuum oven (vacuum degree < 133 Pa) at various temperatures (140, 160, and 180 °C) for different times (2, 5, and 20 h, respectively) and subsequently cooled down to room temperature. All of the samples were homogeneous and optically transparent, and no phase separation was observed.

2.2. Rheological Measurements. The unannealed and annealed films were folded up and compression-molded at 10 MPa and 160 °C into disc samples with a diameter of 25 mm and a thickness of 1.5 mm for rheological testing. The procedure was completed in a short time (5 min) to minimize the influence of compression. The rheological measurements were conducted on an advance rheometric expansion system (ARES-G2, TA, U.S.A.) with parallel plates of 25 mm diameter. Isothermal frequency sweeps were applied in the range of 10^{-2}−10^2 rad/s, and the strain in all measurements was 1%, ensuring that the testing was in the linear viscoelastic region.

2.3. Broadband Dielectric Spectroscopy. Dielectric measurements were performed on a Novocontrol Alpha high-resolution dielectric analyzer (Novocontrol GmbH Concept 40, Novocontrol Technology, Germany), equipped with a Novocool cryogenic system for temperature control with a precision of ±0.1 °C during each sweep. Films of approximately 100 μm thickness were placed between two circular gold electrodes of 20 mm diameter. Isothermal frequency sweeps were carried out over a frequency range of 10^{-1}−10^7 Hz from 0 to 160 °C. Temperature sweeps were conducted at a frequency of 10 Hz and a heating rate of 3 °C/min from 0 to 160 °C.

3. RESULTS AND DISCUSSION

3.1. Molecular entanglement. The entanglement molecular weight M_e, defined as the average molecular weight between adjacent temporary entanglement points, is one of the most fundamental parameters describing the topological network in all tube models. However, it is difficult to obtain the value of M_e in a direct fashion, and it is usually calculated from the plateau modulus G_N^0 (see eq 1), which can be determined by measuring the storage modulus G' and the loss modulus G'' in rheological tests.

$$G_N^0 = \frac{4}{5}\frac{\rho RT}{M_e} \tag{1}$$

in which ρ is the density, R is the gas constant, and T is the absolute temperature. Various semiempirical methods may be used to extract the value of G_N^0, and Liu et al.[35] have made a comparison of these methods. As stated in our previous work,[33] G'' does not exhibit a minimum and a maximum in PMMA/SMA blends. Only tan δ (tan $\delta = G''/G'$) exhibits a minimum. Therefore, the MIN method (see eq 2) suggested by Wu[36−38] is adopted in the present study.

$$G_{N\,exp}^0 = G'(\omega)_{\tan\delta \to \min} \tag{2}$$

In order to cross check the calculated data and achieve a high accuracy, a semiquantitative method based on the crossover modulus G_x ($G_x = G' = G''$ at $\omega = \omega_x$) is also applied.[36]

$$\log\left(\frac{G_N^0}{G_x}\right) = 0.38 + \frac{2.63\log(M_w/M_n)}{1 + 2.45\log(M_w/M_n)} \tag{3}$$

The weight average molecular weight M_w and number average molecular weight M_n for the blends were calculated using

$$M_w = w_1 M_{w1} + w_2 M_{w2} \qquad \frac{1}{M_n} = \frac{w_1}{M_{n1}} + \frac{w_2}{M_{n2}} \tag{4}$$

in which w is the weight fraction and the subscripts 1 and 2 refer to blend components 1 and 2, respectively.

Figure 1 shows the master curves for the unannealed PMMA/SMA (50/50) blend at a reference temperature of 160 °C. One can see that the time−temperature superposition (TTS) principle holds well for the blend. Moreover, typical terminal behavior at low frequencies is observed, $G' \propto \omega^2$ and $G'' \propto \omega$, respectively,[39] which is characteristic of a homogeneous blend structure. The plateau modulus $G_{N\,exp}^0$ was determined using the MIN method in eq 2 and the crossover modulus-based method in eq 3. All relevant parameters are listed in Table 1. It can be seen that $G_{N\,exp}^0$ increases and M_e decreases with increasing annealing temperature and/or time, indicating that the segment packing is in a more compact state and the entanglement density increases after annealing. This occurs because the solution-cast blends are not in thermodynamic equilibrium, and annealing provides a thermodynamic driving force for chain rearrangement and

dx.doi.org/10.1021/jp3098507 | J. Phys. Chem. B 2013, 117, 697−705

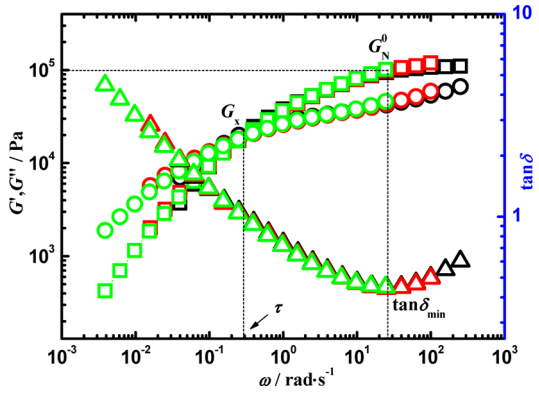

Figure 1. Master curves of the storage modulus (□), loss modulus (○), and loss tangent (Δ) for unannealed PMMA/SMA (50/50) blends at a reference temperature of 160 °C.

increases the efficiency of chain packing. The results obtained from both the MIN method and the crossover modulus-based method exhibit the same trend. However, because the latter is only a semiquantitative method, the data obtained from these two methods are somewhat different, with the crossover modulus-based method being less sensitive to variation.

It is well documented that chain conformations in as-cast thin polymer films are in a nonequilibrium and partially disentangled state.[40−42] Due to the rapid drying of the solvent, the resultant dried films may retain a memory of the chain conformations in the original solution, resulting in a lower entanglement density in the films. Moreover, the entanglement recovery process occurs spontaneously above T_g, as verified by Teng et al.[43], who monitored the re-entanglement kinetics of freeze-dried polystyrene (PS) above T_g. Given this information, we can attribute the increased entanglement density upon annealing to a better efficiency of chain packing and entanglement recovery.

Because all annealed samples actually experience a cooling process to room temperature after high-temperature annealing, it is still not clear whether the increased entanglement density is generated during the annealing process or during the subsequent cooling stage. It is also of interest to determine if an equilibrium entanglement density could be achieved with higher temperatures or longer annealing times. These issues will be dealt with in more detail in the following sections. In addition, two further issues should be pointed out. The first one is that dissimilar chains are generally accepted to be less likely to entangle with each other than with similar chains in polymer blends with dissimilar chain structures.[37] However, because M_e is an average value, inter- and intrachain entanglements cannot be distinguished in this study. The second is that molecular orientation has probably relaxed and attained an equilibrium random state during annealing at such high temperatures and is not considered further here.

3.2. Glass Transition Temperature. The entanglement condition of the chains resulting from various annealing processes differs from those assumed by polymer blends at the entanglement equilibrium, and thus, they may cause different densities and T_g's. Figure 2 shows the corresponding

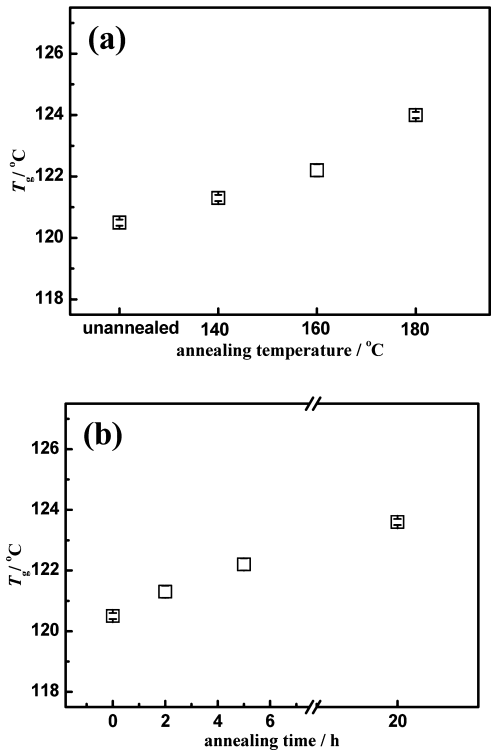

Figure 2. Glass transition temperatures of different annealed PMMA/SMA (50/50) blends detected by dielectric measurements: (a) annealed at different temperatures for 5 h and (b) annealed at 160 °C for different times.

T_g's of PMMA/SMA (50/50) blends annealed at various temperatures for different times. It can be observed that T_g increases with increasing annealing temperature and/or time. Isolated single- and few-chain coils will gradually interpenetrate and re-entangle via thermal diffusion, with the annealing process providing the thermodynamic driving force for chain rearrangement and increasing the efficiency of chain packing. Accordingly, T_g increases due to increased entanglement

Table 1. Plateau Modulus, Crossover Modulus, and Entanglement Molecular Weight for Different Annealed PMMA/SMA (50/50) Blends

annealing					
T (°C)	t (h)	$G_{N\ exp}^0$ (×10^5 Pa)	G_x (×10^4 Pa)	$M_e{}^a$ (×10^{4}g/mol)	$M_e{}^b$ (×10^{4}g/mol)
unannealed		1.07 ± 0.04	1.93 ± 0.04	3.29 ± 0.12	1.94 ± 0.04
140	5	1.18 ± 0.08	2.15 ± 0.19	2.99 ± 0.20	1.75 ± 0.15
	2	1.28 ± 0.06	2.22 ± 0.07	2.75 ± 0.13	1.68 ± 0.05
160	5	1.41 ± 0.09	2.49 ± 0.12	2.50 ± 0.16	1.50 ± 0.07
	20	1.54 ± 0.04	2.65 ± 0.12	2.28 ± 0.06	1.41 ± 0.06
180	5	1.58 ± 0.08	2.70 ± 0.10	2.23 ± 0.11	1.38 ± 0.05

[a]Estimated using the MIN method. [b]Estimated using the crossover modulus-based method.

dx.doi.org/10.1021/jp3098507 | J. Phys. Chem. B 2013, 117, 697−705

density and decreased molecular mobility. This behavior is similar to that found for freeze-dried atactic PS[44] and ultrathin polymer films.[42] However, there is little agreement in the published literature on this subject. Serghei et al.[45] found that no shifts in the glass transition are detected down to film thicknesses of ~10 nm in thin polymer layers having a free upper interface. Tress et al.[46] reported that deviations from the glass transition of the bulk do not exceed ±3 K and are independent of the layer thickness and the molecular weight of the PS under study. Other studies have shown glass transition behavior of polymer films to be affected by the substrate,[47] interfacial conditions,[48] and film thickness.[49] These factors can be ignored in this study because all of the experimental conditions are uniform. One possible cause of change in T_g is that residual solvent in films can act as a plasticizer and decreases T_g.[50] In the present study, the removal of solvent was checked gravimetrically by taking the weight of the films to constant weight and further verified by TGA results (shown in the Supporting Information). No obvious weight loss was observed before the polymers began to decompose for both unannealed and annealed blend films. Therefore, residual solvent is not an issue here. In addition, Kim et al.[51] reported that the T_g of poly(vinyl acetate) (PVAc) increased as a function of annealing time and attributed this to water absorption of PVAc from the ambient atmosphere. However, a stringent drying procedure was employed in this study, and the water absorption of PMMA and SMA was negligible; consequently, the effect of absorbed water can also be neglected. Considering the above facts, the increased T_g is likely to be due to an increased entanglement density in the system.

Because T_g gradually increases and approaches a constant value with increasing annealing temperature and/or time, this indicates the existence of an entanglement equilibrium state. Sauer et al.[52] reported that melt preannealing at $T \gg T_g$ is required to attain an equilibrium entanglement density. In order to make a quantitative comparison, the reptation or longest relaxation time (τ_t) can be calculated using the reptation model[53]

$$D_{rep} \approx Na^2/\tau_t = D_1 N^{-2} \quad (5)$$

in which D_{rep} is the self-diffusion coefficient, N is the degree of polymerization, a is the effective segment length, and D_1 is the monomer friction factor. It is predicted that 6.3×10^5 min at 170 °C is necessary for PS with a M_w of 20000k.[52] However, the diffusion coefficient cannot be easily obtained; therefore, it is difficult to predict the equilibrium time. Also, phase separation or degradation of PMMA/SMA blends may occur when annealed at higher temperatures and/or longer time. Given these uncertainties, it is not possible to establish if an entanglement equilibrium state has been attained in this study.

3.3. Molecular Dynamics. *3.3.1. α-Relaxation Process.* To extract quantitative information from the isothermal dielectric spectra, the imaginary part (dielectric loss) of the complex dielectric function was analyzed in terms of the empirical Havriliak–Negami (HN) function.[54]

$$\varepsilon^* = \varepsilon_\infty + \frac{\Delta\varepsilon}{[1 + (i\omega\tau_{HN})^{\alpha_{HN}}]^{\beta_{HN}}} \quad (6)$$

where ω is angular frequency ($\omega = 2\pi f$), $\Delta\varepsilon$ is the dielectric strength, ε_∞ is the unrelaxed ($\omega = \infty$) value of the dielectric constant, and τ_{HN} is the HN characteristic relaxation time. The exponents α_{HN} and β_{HN} ($0 < \alpha_{HN}, \alpha_{HN}\beta_{HN} \leq 1$) are shape parameters that describe the symmetric and asymmetric broadening of the relaxation time distribution, respectively. In the present case, an additional conductivity was taken into account by adding a term $-i(\sigma/(\varepsilon_0\omega^s))$ to eq 6. Here, σ is the dc conductivity constant, ε_0 is the dielectric permittivity of vacuum, and the coefficient s ($0 < s < 1$) characterizes the conduction mechanism. A conductivity process and two HN functions were used to analyze the isothermal dielectric spectra in this study. Furthermore, τ_{HN} is related to τ_{max} corresponding to the maximum of the dielectric loss by the equation

$$\tau_{max} = \tau_{HN}\left(\sin\frac{\alpha_{HN}\beta_{HN}\pi}{2(\beta_{HN}+1)}\right)^{1/\alpha_{HN}}\left(\sin\frac{\alpha_{HN}\pi}{2(\beta_{HN}+1)}\right)^{-1/\alpha_{HN}} \quad (7)$$

Figure 3 shows the frequency dependences of the dielectric loss ε'' for unannealed PMMA/SMA (50/50) at various

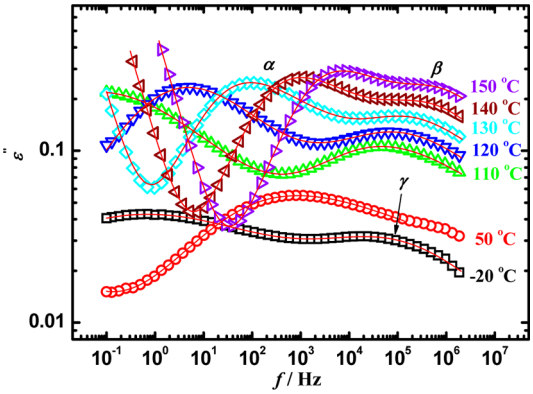

Figure 3. Dielectric loss ε'' as a function of frequency for an unannealed PMMA/SMA (50/50) blend at various temperatures. The solid curves represent HN fits to the data.

temperatures. At lower temperatures, β- and γ-relaxation peaks can be observed. The β-relaxation is connected with partial rotation or conformational changes of the $-COOCH_3$ side groups around the C–C bonds in the main chain of the PMMA component, while the γ-relaxation is connected with rotation of the α-methyl group bonded to the main chain of the PMMA component. Although small amounts of water absorbed from the environment during the preparation of the samples may cause a similar result,[55] the samples in this work have been so well dried that this possibility can be excluded. At higher temperatures (130–150 °C), two relaxation processes, α and β plus ionic conductivity, can be observed. The α-relaxation is associated with segmental motion of the blends. For the annealed blends, the frequency–temperature dependences of ε'' are similar and are not shown.

In order to clarify the effect of annealing on the α-relaxation, Figure 4 shows the normalized ε'' at 130 °C of different annealed PMMA/SMA (50/50) blends. It can be seen that the α-relaxation peak shifts to lower frequencies after annealing, suggesting that the α-relaxation time increases. This result is similar to that reported for annealed ultrathin Al-supported PVAc films.[19] As discussed above, the influence of annealing on the α-relaxation dynamics of PMMA/SMA blends is correlated to increased entanglement density and decreased molecular mobility. To make quantitative comparisons between them, Figure 5 shows τ_{max} of the α-relaxation as a function of

dx.doi.org/10.1021/jp3098507 | J. Phys. Chem. B 2013, 117, 697–705

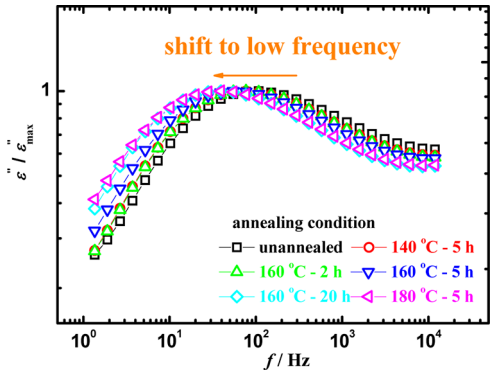

Figure 4. Dielectric loss ε'' of different annealed PMMA/SMA (50/50) blends measured at 130 °C. The data have been normalized to the maximum and rescaled for clarity.

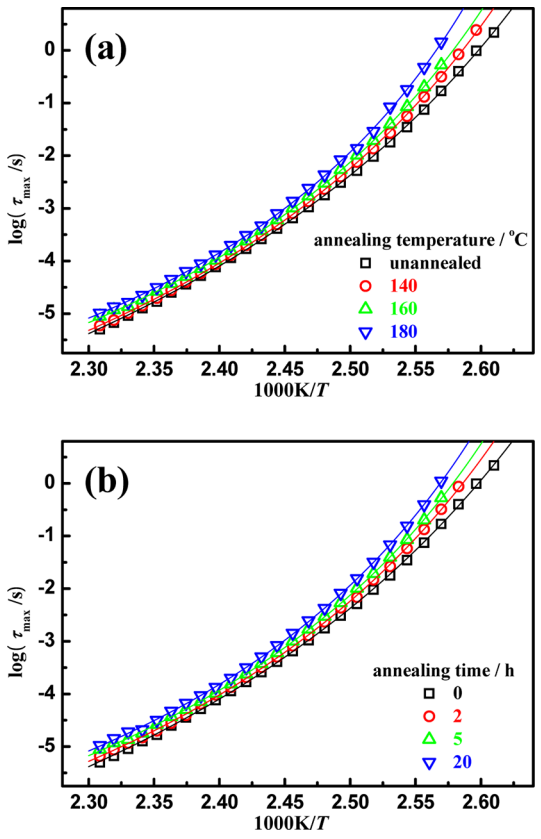

Figure 5. Relaxation time of the α-relaxation process as a function of temperature for different annealed PMMA/SMA (50/50) blends: (a) annealed at different temperatures for 5 h and (b) annealed at 160 °C for different times. The solid curves represent VFT fits to the data.

temperature for unannealed and different annealed PMMA/SMA (50/50) blends. It is obvious that τ_{max} increases with increasing annealing temperature and/or time, indicating a decreased α-relaxation rate. Because annealing provides a thermodynamic driving force for chain rearrangement and increases the efficiency of chain packing, the entanglement density increases, and the molecular mobility decreases. Hence, the α-relaxation peak shifts to lower frequency, and the relaxation rate decreases. Moreover, with increasing annealing temperature and/or time, the increase of τ_{max} gradually slows down, indicating that further annealing seems to approach an entanglement equilibrium state, and an equilibrium relaxation time appears. This result is consistent with the T_g results reported above. On the basis of this evidence, it suggests that an equilibrium entanglement density can indeed be achieved when melt annealing at $T \gg T_g$. In the latest finding reported by Boucher et al.,[56] T_g decreased with decreasing film thickness, whereas intrinsic molecular dynamics were independent of the film thickness in PS thin films. They attributed this result to the fact that the molecular mobility and T_g were affected differently by geometrical factors.

The samples in this study have undergone a two-step thermal treatment, annealing at high temperature followed by cooling to room temperature. Whether the increased entanglement density was generated during the annealing process or in the subsequent cooling procedure is still not clear. Hence, another experiment was conducted as follows: the first frequency sweep was carried out at a predetermined temperature and then kept isothermally for 2 h at the identical temperature; subsequently, the second frequency sweep at the same temperature was done without cooling down to room temperature. Figure 6 shows

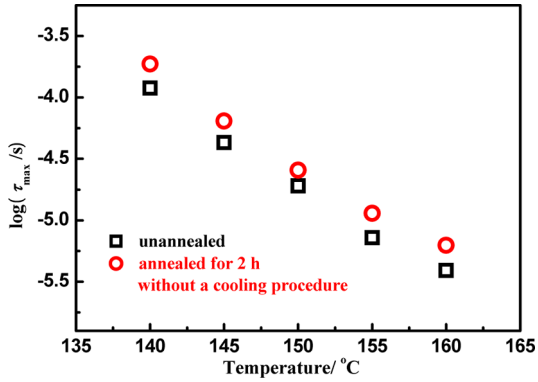

Figure 6. α-Relaxation time of unannealed and annealed at corresponding temperatures for PMMA/SMA (50/50) blends under various temperatures, which never experienced a cooling procedure.

τ_{max} of the α-relaxation as a function of temperature for unannealed and annealed PMMA/SMA blends without the cooling treatment. It can be observed that τ_{max} increases after 2 h of annealing due to increased entanglement density, indicating that the increase in entanglement density occurs during the annealing process rather than the subsequent cooling procedure.

The temperature dependences of τ_{max} corresponding to the α-relaxation can be well described by the empirical Vogel–Fulcher–Tamman (VFT) equation

$$\log \tau_{max} = \log \tau_0 + \frac{A}{T - T_0} \quad (8)$$

where τ_0 is the relaxation time at infinite temperature, A is related to the fragility of the system, which can also be written as DT_0, D is the fragility strength parameter,[57] and T_0 is the so-called Vogel temperature or ideal glass transition temperature, which is typically 30–70 K lower than T_g. The parameters, obtained from the fittings of the VFT equation to τ_{max} of Figure 5, are presented in Table 2. It can be seen that τ_0 increases with increasing annealing temperature and/or time, while the fragility parameter A decreases, suggesting that the fragility of the system increases. The Vogel temperature T_0 shows a similar dependence on the annealing temperature and/or time as T_g. These results are in good agreement with the relaxation time

dx.doi.org/10.1021/jp3098507 | J. Phys. Chem. B 2013, 117, 697–705

Table 2. Relevant Fitting Parameters for the VFT Equation for Different Annealed PMMA/SMA (50/50) Blends

annealing				
T (°C)	t (h)	log τ_0 (s)	A (K)	T_0 (K)
unannealed		−12.0 ± 0.1	728.4 ± 20.2	324.0 ± 1.0
140	5	−11.2 ± 0.1	591.7 ± 16.9	333.8 ± 0.9
	2	−11.0 ± 0.2	573.2 ± 22.3	334.6 ± 1.3
160	5	−10.4 ± 0.1	496.8 ± 14.1	340.1 ± 0.9
	20	−10.2 ± 0.1	464.7 ± 13.6	343.7 ± 0.9
180	5	−9.8 ± 0.2	413.6 ± 21.5	347.6 ± 1.4

τ_{max} and T_g values reported above. On the basis of these results, one can conclude that due to the increased entanglement density and decreased molecular mobility, the α-relaxation time and the fragility of PMMA/SMA blends increase while the relaxation rate decreases with increasing annealing temperature and/or time.

As observed in Figure 3, PMMA/SMA (50/50) blends exhibit two relaxation processes (α- and β-relaxation) in the investigated frequency range at high temperatures (>110 °C). The mechanism of annealing may be deduced by quantitatively analyzing the changes of the relaxation time distribution $G(\tau)$ under various annealing temperatures and times. Figure 7 shows $G(\tau)$ curves for α- and β-relaxation at 130 °C for PMMA/SMA (50/50) blends with different annealing treatments. The peaks with longer relaxation time scales are the α-relaxation, and the shorter ones correspond to the β-relaxation. It can be observed that the relaxation modes of the α-relaxation shift to a longer average relaxation time with increasing annealing temperature and/or time, meaning that the α-relaxation time increases and the relaxation rate decreases. The changes in the relaxation time distribution of the α-relaxation are consistent with shifts in the mean values of τ_{max} and the position of the α-relaxation peak (T_g) discussed above. Meanwhile, the relaxation peak height monotonically decreases with increasing annealing temperature and/or time, indicating that the relative number of relaxing elements decreases, which is consistent with decreasing chain mobility due to increasing entanglement density. However, no obvious distribution broadening is observed for the α-relaxation, although the distributions shift to longer relaxation times. On the other hand, the β-relaxation modes are hardly affected by annealing. This will be discussed in detail later.

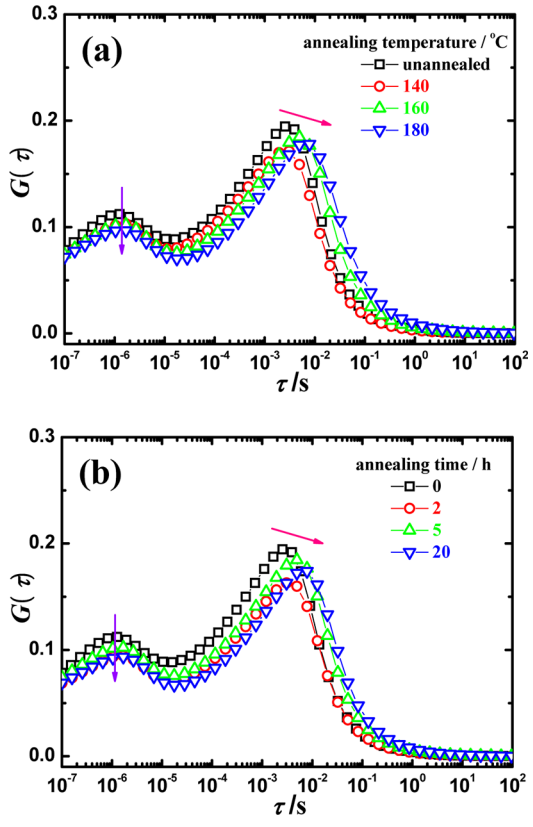

Figure 7. Relaxation time distribution of different annealed PMMA/SMA (50/50) blends at 130 °C: (a) annealed at different temperatures for 5 h and (b) annealed at 160 °C for different times.

The effect of annealing on the shape parameters of the α-relaxation peak was also analyzed. The relaxation peak shape is associated with segmental dynamics and is mainly affected by heterogeneity. Figure 8 gives the shape parameters of the α-relaxation peaks at 130 °C for different annealed PMMA/SMA (50/50) blends. It can be observed that the α_{HN} and β_{HN} values are almost unchanged when the annealing temperature and/or time increases, suggesting that the width and symmetry of the α-relaxation spectra are hardly affected by annealing temperature and/or time. This differs from the results found in ultrathin polymer films.[19,58] The almost unchanging relaxation spectra shape can be attributed to unchanged heterogeneous dynamics, although the entanglement density increases for the annealed samples.

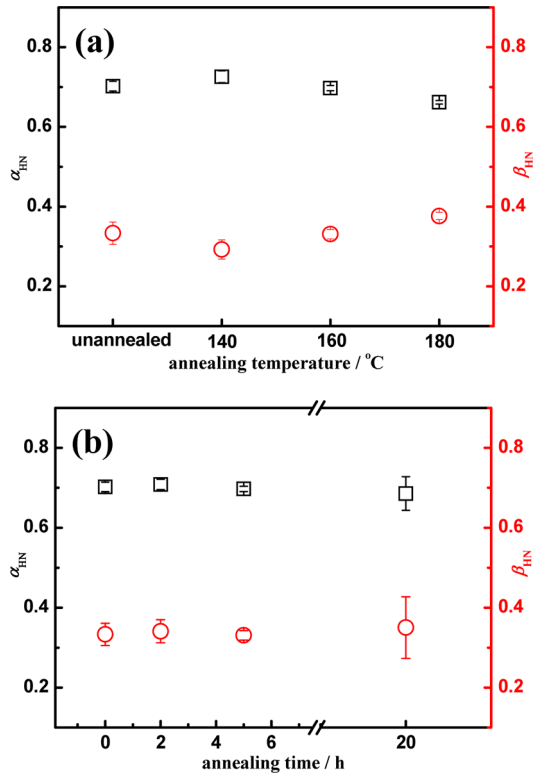

Figure 8. Shape parameters of the α-relaxation as a function of annealing temperature and time for PMMA/SMA (50/50) blends at 130 °C: (a) annealed at different temperatures for 5 h and (b) annealed at 160 °C for different times.

Figure 9 shows the frequency dependences of ε'' normalized by the peak values for different annealed PMMA/SMA (50/50)

dx.doi.org/10.1021/jp3098507 | J. Phys. Chem. B 2013, 117, 697−705

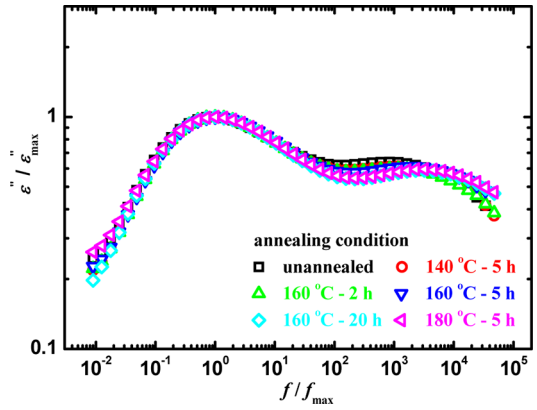

Figure 9. Normalized frequency dependences of dielectric loss ε'' for the α-relaxation processes of different annealed PMMA/SMA (50/50) blends at 130 °C.

blends at 130 °C. Because these annealed samples present different α-relaxation times, the β-relaxation peaks of annealed samples will shift to higher frequencies when the α-relaxation peaks are normalized. Moreover, it can be seen that the width and symmetry of the α-relaxation spectra are almost unchanged by annealing temperature and/or time, which is in good agreement with the shape parameters, as shown in Figure 8. These results further confirm that although the entanglement density increased and the molecular mobility decreased with the increase of annealing temperature and/or time, heterogeneous dynamics are almost unchanged.

3.3.2. β- and γ-Relaxation Processes. As mentioned earlier, for PMMA/SMA blends, the β-relaxation is connected with partial rotation or conformational changes of the $-COOCH_3$ side groups around the C−C bonds in the main chain of the PMMA component, while the γ-relaxation is connected with rotation of the α-methyl group bonded to the main chain of the PMMA component. In order to further investigate the effect of annealing on subglass relaxation (β- and γ-relaxation) processes, the temperature dependences of τ_{max} corresponding to the peaks of the β- and γ-relaxation processes are plotted in Figure 10. All β- and γ-relaxation processes follow an Arrhenius behavior, which is characteristic of subglass relaxation processes

$$\tau_{max} = \tau_0 \exp\left(\frac{E_a}{RT}\right) \quad (9)$$

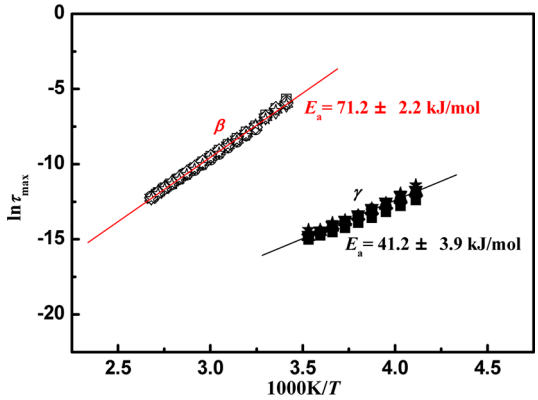

Figure 10. Activation plots for the β-relaxation (open symbols) and γ-relaxation (solid symbols) processes of different annealed PMMA/SMA (50/50) blends.

where τ_0 is the high-temperature limit of the relaxation time, R is the gas constant, and E_a (kJ/mol) is the activation energy, which can be obtained from the slopes. It can be noted that the activation energies of the β- and γ-relaxation processes seem to be independent of the annealing temperature and/or time, and the values are 71.2 ± 2.2 and 41.2 ± 3.9 kJ/mol, respectively, indicating that the dynamics of subglass relaxation processes are scarcely affected by annealing. The activation energy of the β-relaxation for the PMMA/SMA blend is slightly lower than that of pure PMMA[55,59] due to the strong intermolecular interactions between the phenyl groups in SMA and carbonyl groups in PMMA,[60] which leads to an increase of mobility and consequently to the decrease of E_a. The value is in good agreement with our previous work.[33]

Figure 11 shows the normalized curves of the β-relaxation process for different annealed PMMA/SMA blends at 50 °C. It

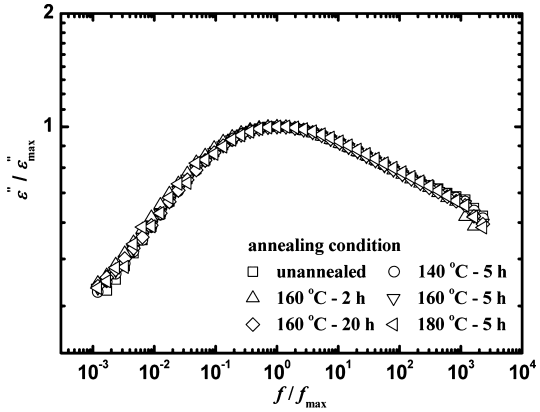

Figure 11. Normalized frequency dependences of dielectric loss ε'' for the β-relaxation processes of different annealed PMMA/SMA (50/50) blends at 50 °C.

can be clearly seen that the distribution width of the β-relaxation is almost independent of annealing temperature and/or time. On the basis of these results, one can conclude that neither the dynamics nor the distribution width of the subglass relaxation processes is affected by annealing, indicating that the local environment of the segments is not changed. Moreover, these results further confirm that different molecular entanglement densities do not affect subglass relaxation dynamics and distribution, similar to our previous results.[33] These results can be interpreted as follows: The subglass relaxation is a local element (side or functional groups) relaxation mode. Accordingly, rotational motion can be freely attained without overcoming chain entanglement resistance. Hence, neither the dynamics nor the distribution width of the subglass relaxation processes is affected by the chain entanglement density. However, in the case of the pure PMMA component, although the peak frequency (and thus τ_{max}) is essentially unchanged, the β-relaxation peak becomes narrower at the low-frequency side, and the overlap of the α- and β-relaxation diminishes during physical aging,[55,59] which somewhat differs from the situation in the PMMA/SMA blends under investigation.

4. CONCLUSIONS

The chain entanglement density of PMMA/SMA blends increases when the annealing temperature and/or time increases, and the increased entanglement density results from the annealing process rather than the subsequent cooling

dx.doi.org/10.1021/jp3098507 | J. Phys. Chem. B 2013, 117, 697−705

procedure. Moreover, an equilibrium entanglement density can be achieved when melt annealing at $T \gg T_g$. Increased chain entanglement density resulting from annealing has a pronounced effect on segmental motion, including the relaxation transition temperature (T_g) and segmental dynamics. T_g shifts to higher temperatures, and the relaxation time τ_{max} increases with increasing annealing temperature and/or time. It is further found that the Vogel temperature and the fragility of the system increase. However, no obvious distribution broadening is observed. Due to the particular characteristics of the mobile elements of the subglass relaxation, rotational motion can be freely achieved without overcoming the chain entanglement resistance. Hence, neither the dynamics nor the distribution width of the subglass relaxation (β- and γ-relaxation) processes is affected by chain entanglement, indicating that the local environment of the segments is not changed.

■ ASSOCIATED CONTENT

Supporting Information

Thermogravimetry measurements of unannealed and annealed polymer blend films. This material is available free of charge via the Internet at http://pubs.acs.org.

■ AUTHOR INFORMATION

Corresponding Author

*Tel./Fax: +86 571 8795 2522. E-mail: shangguan@zju.edu.cn; zhengqiang@zju.edu.cn.

Notes

The authors declare no competing financial interest.

■ ACKNOWLEDGMENTS

This work was supported by the National Nature Science Foundation of China (No. 51173165), the Nature Science Foundation of Zhejiang Province (No. Y4100314), and the Program for Zhejiang Provincial Innovative Research Team (No. 2009R50004).

■ REFERENCES

(1) Frank, C. W.; Rao, V.; Despotopoulou, M. M.; Pease, R. F. W.; Hinsberg, W. D.; Miller, R. D.; Rabolt, J. F. *Science* **1996**, *273*, 912−915.
(2) Heriot, S. Y.; Jones, R. A. L. *Nat. Mater.* **2005**, *4*, 782−786.
(3) Kim, J. S.; Ho, P. K. H.; Murphy, C. E.; Friend, R. H. *Macromolecules* **2004**, *37*, 2861−2871.
(4) Nilsson, S.; Bernasik, A.; Budkowski, A.; Moons, E. *Macromolecules* **2007**, *40*, 8291−8301.
(5) Hutchinson, J. M. *Prog. Polym. Sci.* **1995**, *20*, 703−760.
(6) Affrossman, S.; O'Neill, S. A.; Stamm, M. *Macromolecules* **1998**, *31*, 6280−6288.
(7) Ton-That, C.; Shard, A. G.; Daley, R.; Bradley, R. H. *Macromolecules* **2000**, *33*, 8453−8459.
(8) Harris, M.; Appel, G.; Ade, H. *Macromolecules* **2003**, *36*, 3307−3314.
(9) Malchev, P. G.; de Vos, G.; Norder, B.; Picken, S. J.; Gotsis, A. D. *Polymer* **2007**, *48*, 6294−6303.
(10) Bell, J. R.; Chang, K.; Lopez-Barron, C. R.; Macosko, C. W.; Morse, D. C. *Macromolecules* **2010**, *43*, 5024−5032.
(11) Zheng, L. D.; Liu, J. G.; Ding, Y.; Han, Y. C. *J. Phys. Chem. B* **2011**, *115*, 8071−8077.
(12) Chen, R. F.; Shangguan, Y. G.; Zhang, C. H.; Chen, F.; Harkin-Jones, E.; Zheng, Q. *Polymer* **2011**, *52*, 2956−2963.
(13) Ran, X. H.; Jia, Z. Y.; Han, C. Y.; Yang, Y. M.; Dong, L. S. *J. Appl. Polym. Sci.* **2010**, *116*, 2050−2057.
(14) Takayama, T.; Todo, M.; Tsuji, H. *J. Mech. Behav. Biomed.* **2011**, *4*, 255−260.
(15) Liang, Y. L.; Moghbelli, E.; Sue, H. J.; Minkwitz, R.; Stark, R. *Polymer* **2012**, *53*, 604−612.
(16) Marchese, P.; Celli, A.; Fiorini, M.; Gabaldi, M. *Eur. Polym. J.* **2003**, *39*, 1081−1089.
(17) Lu, S. X.; Cebe, P. *Polymer* **1996**, *37*, 4857−4863.
(18) Ruderer, M. A.; Prams, S. M.; Rawolle, M.; Zhong, Q.; Perlich, J.; Roth, S. V.; Muller-Buschbaum, P. *J. Phys. Chem. B* **2010**, *114*, 15451−15458.
(19) Nguyen, H. K.; Labardi, M.; Capaccioli, S.; Lucchesi, M.; Rolla, P.; Prevosto, D. *Macromolecules* **2012**, *45*, 2138−2144.
(20) Kong, M. Q.; Huang, Y. J.; Chen, G. L.; Yang, Q.; Li, G. X. *Polymer* **2011**, *52*, 5231−5236.
(21) Tan, Y. Q.; Yin, X. Z.; Chen, M. T.; Song, Y. H.; Zheng, Q. *J. Rheol.* **2011**, *55*, 965−979.
(22) Malchev, P. G.; Norder, B.; Picken, S. J.; Gotsis, A. D. *Polymer* **2007**, *48*, 6834−6842.
(23) Hodge, I. M. *Science* **1995**, *267*, 1945−1947.
(24) Hodge, I. M.; Berens, A. R. *Macromolecules* **1982**, *15*, 762−770.
(25) Simon, S. L.; Sobieski, J. W.; Plazek, D. J. *Polymer* **2001**, *42*, 2555−2567.
(26) Boucher, V. M.; Cangialosi, D.; Alegria, A.; Colmenero, J.; Pastoriza-Santos, I.; Liz-Marzan, L. M. *Soft Matter* **2011**, *7*, 3607−3620.
(27) Cangialosi, D.; Boucher, V. M.; Alegria, A.; Colmenero, J. *J. Chem. Phys.* **2011**, *135*, 014901.
(28) Chopra, D.; Kontopoulou, M.; Vlassopoulos, D.; Hatzikiriakos, S. G. *Rheol. Acta* **2002**, *41*, 10−24.
(29) Vlassopoulos, D. *Rheol. Acta* **1996**, *35*, 556−566.
(30) Yu, W.; Li, R. M.; Zho, C. X. *Polymer* **2011**, *52*, 2693−2700.
(31) Li, R. M.; Yu, W.; Zhou, C. X. *Polym. Bull.* **2006**, *56*, 455−466.
(32) Lin, Y.; Shangguan, Y. G.; Chen, F.; Zuo, M.; Zheng, Q. *Polym. Int.* **2013**, DOI: 10.1002/pi.4349.
(33) Lin, Y.; Shangguan, Y. G.; Zuo, M.; Harkin-Jones, E.; Zheng, Q. *Polymer* **2012**, *53*, 1418−1427.
(34) Bergman, R.; Alvarez, F.; Alegria, A.; Colmenero, J. *J. Chem. Phys.* **1998**, *109*, 7546−7555.
(35) Liu, C. Y.; He, J. S.; van Ruymbeke, E.; Keunings, R.; Bailly, C. *Polymer* **2006**, *47*, 4461−4479.
(36) Wu, S. H. *J. Polym. Sci., Part B: Polym. Phys.* **1989**, *27*, 723−741.
(37) Wu, S. H. *J. Polym. Sci., Part B: Polym. Phys.* **1987**, *25*, 557−566.
(38) Wu, S. H.; Beckerbauer, R. *Polymer* **1992**, *33*, 509−515.
(39) Ferry, J. D. *Viscoelastic Properties of Polymers*, 3rd ed.; John Willey & Sons: New York, 1980.
(40) Raegen, A.; Chowdhury, M.; Calers, C.; Schmatulla, A.; Steiner, U.; Reiter, G. *Phys. Rev. Lett.* **2010**, *105*, 227801.
(41) Li, R. N.; Clough, A.; Yang, Z. H.; Tsui, O. K. C. *Macromolecules* **2012**, *45*, 1085−1089.
(42) Napolitano, S.; Wubbenhorst, M. *Nat. Commun.* **2011**, *2*, 260.
(43) Teng, C.; Gao, Y.; Wang, X. L.; Jiang, W.; Zhang, C.; Wang, R.; Zhou, D. S.; Xue, G. *Macromolecules* **2012**, *45*, 6648−6651.
(44) Rong, W. R.; Fan, Z. Y.; Yu, Y.; Bu, H. S.; Wang, M. *J. Polym. Sci., Part B: Polym. Phys.* **2005**, *43*, 2243−2251.
(45) Serghei, A.; Huth, H.; Schick, C.; Kremer, F. *Macromolecules* **2008**, *41*, 3636−3639.
(46) Tress, M.; Erber, M.; Mapesa, E. U.; Huth, H.; Muller, J.; Serghei, A.; Schick, C.; Eichhorn, K. J.; Volt, B.; Kremer, F. *Macromolecules* **2010**, *43*, 9937−9944.
(47) Erber, M.; Tress, M.; Mapesa, E. U.; Serghei, A.; Eichhorn, K. J.; Voit, B.; Kremer, F. *Macromolecules* **2010**, *43*, 7729−7733.
(48) Serghei, A.; Tress, M.; Kremer, F. *J. Chem. Phys.* **2009**, *131*, 154904.
(49) Fryer, D. S.; Peters, R. D.; Kim, E. J.; Tomaszewski, J. E.; de Pablo, J. J.; Nealey, P. F.; White, C. C.; Wu, W. L. *Macromolecules* **2001**, *34*, 5627−5634.
(50) Serghei, A.; Kremer, F. *Macromol. Chem. Phys.* **2008**, *209*, 810−817.

(51) Kim, S.; Mundra, M. K.; Roth, C. B.; Torkelson, J. M. *Macromolecules* **2010**, *43*, 5158−5161.
(52) Sauer, B. B.; Walsh, D. J. *Macromolecules* **1994**, *27*, 432−440.
(53) de Gennes, P. G.. *Scaling Concepts in Polymer Physics*; Cornell University Press: Ithaca, NY, 1979.
(54) Havriliak, S.; Negami, S. *Polymer* **1967**, *8*, 161−210.
(55) Wypych, A.; Duval, E.; Boiteux, G.; Ulanski, J.; David, L.; Mermet, A. *Polymer* **2005**, *46*, 12523−12531.
(56) Boucher, V. M.; Cangialosi, D.; Yin, H. J.; Schonhals, A.; Alegria, A.; Colmenero, J. *Soft Matter* **2012**, *8*, 5119−5122.
(57) Richert, R.; Angell, C. A. *J. Chem. Phys.* **1998**, *108*, 9016−9026.
(58) Nguyen, H. K.; Prevosto, D.; Labardi, M.; Capaccioli, S.; Lucchesi, M.; Rolla, P. *Macromolecules* **2011**, *44*, 6588−6593.
(59) Casalini, R.; Roland, C. M. *J. Non-Cryst. Solids* **2011**, *357*, 282−285.
(60) Feng, H. Q.; Shen, L. F.; Feng, Z. L. *Eur. Polym. J.* **1995**, *31*, 243−247.